# PCCP

Accepted Manuscript

Volume 1 | Number 1 | Jan 2013 | Pages 1–100
PCCP
Physical Chemistry Chemical Physics
www.rsc.org/pccp
ROYAL SOCIETY OF CHEMISTRY

This is an *Accepted Manuscript*, which has been through the Royal Society of Chemistry peer review process and has been accepted for publication.

*Accepted Manuscripts* are published online shortly after acceptance, before technical editing, formatting and proof reading. Using this free service, authors can make their results available to the community, in citable form, before we publish the edited article. We will replace this *Accepted Manuscript* with the edited and formatted *Advance Article* as soon as it is available.

You can find more information about *Accepted Manuscripts* in the Information for Authors.

Please note that technical editing may introduce minor changes to the text and/or graphics, which may alter content. The journal's standard Terms & Conditions and the Ethical guidelines still apply. In no event shall the Royal Society of Chemistry be held responsible for any errors or omissions in this *Accepted Manuscript* or any consequences arising from the use of any information it contains.

ROYAL SOCIETY OF CHEMISTRY

www.rsc.org/pccp

PCCP RSCPublishing

ARTICLE

Cite this: DOI: 10.1039/x0xx00000x

Received 00th January 2012,
Accepted 00th January 2012

DOI: 10.1039/x0xx00000x

www.rsc.org/

# The weak, fluctuating, dipole moment of membrane-bound hydrogenase from *Aquifex aeolicus* accounts for its adaptability to charged electrodes

Francesco Oteri[a], Alexandre Ciaccafava[b], Anne de Poulpiquet[b], Marc Baaden[a], Elisabeth Lojou[b] and Sophie Sacquin-Mora[a]

[NiFe] hydrogenases from *Aquifex aeolicus* (AaHase) and *Desulfovibrio fructosovorans* (DfHase) have been mainly studied to characterize physiological electron transfer processes, or to develop biotechnological devices such as biofuel cells. In this context, it remains difficult to control the orientation of AaHases on electrodes to achieve a fast interfacial electron transfer. Here, we study the electrostatic properties of these two proteins based on microsecond-long molecular dynamics simulations that we compare to voltammetry experiments. Our calculations show weak values and large fluctuations of the dipole direction in AaHase compared to DfHase, enabling the AaHase to absorb on both negatively and positively charged electrodes, with an orientation distribution that induces a spread in electron transfer rates. Moreover, we discuss the role of the transmembrane helix of AaHase and show that it does not substantially impact the general features of the dipole moment.

## Introduction

Because of their ability to reversibly cleave hydrogen into protons and electrons in several organisms,[1-3] hydrogenases (Hases) are particularly interesting enzymes in the field of green economy, grafted on anodes for biofuel cells,[4, 5] or for bio-hydrogen production.[6] We focused this study on the electricity production and, among the different kinds of Hases (see ref.[2] for a review on Hase classification), we selected the [NiFe] Hases from *Desulfovibrio fructosovorans* (DfHase) and *Aquifex aeolicus* (AaHase). The former is soluble, mesophilic and inactivated by $O_2$ and CO while the latter is a membrane-bound Hase (MBH), thermophilic and $O_2$- CO- tolerant.[7-9] In particular we attempt to explain how the enzymes' electrostatic features drive the association characteristics of DfHase[10] and AaHase[4, 9, 11, 12] on charged electrodes.

[NiFe] Hases are composed of two subunits (large and small, see Fig.1a). The large subunit hosts the active site, while the small one contains three iron-sulfur clusters called, relative to the active site, proximal, medial and distal. The proximal cluster is either a [4Fe4S] cubane cluster in soluble Hases or a [4Fe3S] one coordinated by six cysteines in $O_2$-tolerant MBHs (Fig. SI1B).[13-20] The medial cluster is a [3Fe4S] cluster, while the distal one is a [4Fe4S] coordinated by 3 cysteines and one histidine (Fig. SI1C). Because of this arrangement, the three clusters act like a wire transporting the electrons from the active site to the biological partner. In addition, MBHs have a trans-membrane helix at the C-terminus of the small subunit as identified by mass spectroscopy[11] and elucidated by the structure of a related Hase from *E. coli*.

The Lojou group used AaHase to develop a powerful biofuel cell.[4] However, several challenges regarding the protein-electrode interaction have been identified that are crucial for further improvement in the biofuel cell performances. Compared to usual platinum catalysts, the orientation of the biocatalyst on the electrode controls the rate of the electron transfer. If the enzyme is oriented with the distal FeS cluster at a tunneling distance of the electrochemical interface, fast direct electron transfer (DET) is observed. Conversely, if the distal cluster is too far from the electrode, a redox chemical mediator is needed as a shuttle to drive the electrons from the enzyme to the electrode, resulting in mediated electron transfer (MET). Experiments with a functionalized gold electrode showed that using DfHase results in a DET/(DET+MET)-ratio close to 1 on positive surfaces and 0 using a negative surface.[10] A different behavior is observed using AaHase, which results in a DET/(DET+MET)-ratio close to 0.5 independently of the charge of the self-assembled monolayer (SAM) used to immobilize the enzyme on the electrode,[4] thus indicating that AaHase can adopt various orientations on the surface.[12] Besides, the interaction with the detergent has also been found to influence the enzyme orientation, favoring mediated electron transfer on hydrophobic SAMs.[12]

## Experimental section

### Voltammetry

Df and Aa Hases were purified as previously described.[9] Poly(L-lysine) hydrobromide (Mw 15,000-30,000) (PLL) was obtained from Sigma. Poly(L-glutamic) acid sodium salt (Mw 50,000) (PLG) was obtained from ICN Biomedicals Inc. Experiments were performed under $H_2$ atm. in 50 mM HEPES buffer pH 7.2 at 25°C and 60°C for Df and Aa Hases respectively. Cyclic voltammetry was carried out using a PARSTAT 2273 potentiostat from Princeton Applied Research (PAR). A conventional three-electrode system was used with an Ag/AgCl/NaCl (sat.) reference electrode and a platinum wire as auxiliary electrode. Temperature of the electrochemical cell was regulated using a water bath. The reference electrode was separated from the electrolyte using a side junction maintained at room temperature. All potentials are quoted against the Ag/AgCl reference. The working electrode was constructed from a pyrolytic graphite disk ($A = 7$ $mm^2$), polished with 0.05 µm alumna, and then rinsed with ethanol then water. 30 µM PLL and PLG solutions in water were used for PG electrode modification, yielding positively and negatively charged surfaces, respectively. After rinsing in water, 2 µl of 10 µM hydrogenase was applied to the surface of the electrode until drying. The bioelectrode was rinsed in Hepes buffer before running electrochemistry experiments to remove weakly adsorbed enzymes.

### Computational Methods

The wild type DfHase crystal structure (PDB 1FRF) has been used as the starting structure for the DfHase simulation, while comparative homology modeling was used to build a starting structure for AaHase with MODELLER v9.1.[21, 22] Both systems were then simulated using GROMACS 4.5.3[23] and dipole moments were calculated through the Dipole Watcher VMD Plugin. More detailed information regarding the simulations is available as Supporting Information.

## Results and Discussion

The importance of the electrostatic interaction between protein and electrode has been recently highlighted through modeling and SEIRA spectroscopy,[24] where the charge of the electrode was modulated by varying the protonation level of the SAM. Highly ionized SAMs were found to lead to stronger adsorption of the hydrogenase.[24] In the present paper, we used 2-microsecond-long Molecular Dynamics simulations to investigate the electrostatic properties of the two proteins (See Supporting Information for details on the methodology). The electrostatic potential of the two molecules is reported in Fig. SI2 and shows several marked electrostatic spots. In AaHase five negative spots are observed, while only two negative lobes are present on the small subunit of DfHase. The biggest lobe (A) lies on top of the distal FeS cluster while the second largest one (B) is located at the borderline between the two subunits. It has been demonstrated that, as a general feature of the $O_2$-sensitive Hases,[25] a negative spot (A in Fig. SI2) promotes the correct orientation of DfHase with respect to its association partner.[26] AaHase, on the other hand, lacks such a spot at the pH of the simulations (7), which results in significant differences in the magnitude of the dipole moment (Fig. SI3).

In this work, instead of modifying a gold electrode by thiol monolayers, we used a pyrolytic graphite (PG) electrode covered by a layer of charged polyelectrolytes, thus providing a charged surface for the electrode.[27, 28] Figure 2 shows the average voltammograms over three experiments recorded for AaHase and DfHase under $H_2$ atmosphere. Despite current variability each experiment presented the same trend: using AaHase (Fig. 2a), the generated current for catalytic $H_2$ oxidation is higher than the one generated using the bare PG electrode regardless of the charge of the electrode. In contrast, DfHase (Fig. 2b) produces less current at a negatively charged than at the bare or positively charged electrode. The magnitude of the current for $H_2$ oxidation is linked to the number of immobilized enzymes and their orientation towards the surface. The bare PG electrode itself is negatively charged because of the graphite surface's low pKa (around 5).[29] The recovered enzyme activity is linked to the microporosity of the polished graphite surface that permits to partly overcome an orientation limitation.[12] The polyelectrolytes used to modify the electrode surface induce an increase in the charged interacting sites for the enzyme and also probably diminish the microporosity. Accordingly, the orientation of the enzyme limits the interfacial electron transfer. Hence, far less DfHase would be positioned in a favorable orientation for $H_2$ oxidation on a negatively charged electrode. In the case of AaHase, the enzyme orientation distribution presents similar proportions of correctly oriented enzymes regardless of the polyelectrolyte charge, although with a lesser ratio for the negatively charged electrode.

To explain this phenomenon, which is in agreement with the previous findings at SAM-modified gold electrodes,[10, 12] the enzyme dipole moment has been monitored during MD simulations and, since its strength remains stable along time (Fig. SI3), we focused on its directional fluctuations expressed as a function of the angles θ and φ (Fig. 1b). A φ value of 0° corresponds to a dipole moment pointing toward the $Mg^{2+}$ ion, and for $\theta=0°$ the dipole moment is directed opposite to the distal FeS cluster. As a consequence, for θ belonging to the $0° \rightarrow 90°$ range, the negative part of the dipole moment lies around the distal FeS cluster, thus favoring its binding onto positively charged electrodes. On the other hand, for θ values in the $90° \rightarrow 180°$ range, the dipole moment points toward the distal FeS cluster, thus favoring its vicinity to negatively charged electrodes. However, the actual (θ,φ) range for successful electrode binding is likely tighter because not all configurations with a favorable dipole direction are able to position the distal FeS cluster close enough to the surface for DET. For DfHase, the dipole moment presents a strength of about 1200 D, which is similar to values previously obtained for other *Desulfovibrio* $O_2$-sensitive hydrogenases,[24, 30] and its direction feebly fluctuates around the (45°,120°) value pair (see Fig. 3a), thus staying close to its direction in the crystal structure.[10] This low value of θ favors the positioning of the distal FeS cluster on a positively charged electrode, which is in agreement with the cyclic voltammetry experiments presented earlier (see Fig. 2b), and with experiments made on gold modified electrodes.[10] On the other hand, the AaHase dipole moment presents a reduced strength of about 200 D and large variations of its (θ,φ) values. However, the distribution for θ lies for its greater part in the $0° \rightarrow 90°$ range, thus suggesting more efficient binding on positively charged electrodes than on negatively charged ones. Again this result is in agreement with the electrochemical experiments, since electrodes coated with poly-L-lysine lead to higher currents than those coated with poly-glutamate (see Fig. 2a). Previous experiments with thiol monolayers coated gold electrodes also showed higher DET/(DET +MET)-ratios on positively charged, cysteamine modified, surfaces than on negatively charged, mercaptopropionic acid modified, ones.[9] Overall, it seems that both proteins developed different strategies for partner binding : while in DfHase the electrostatic interactions with the redox partner play a crucial role, thus resulting in a strong and stable protein dipole moment; this property is not required for AaHase, which presents a weak and fluctuating dipole moment, but can rely on its transmembrane helix for anchorage.

To further investigate these variations in the dipole moment direction, we calculated the dipole moments for each subunit separately (Fig. SI4) and their angle during the simulation (Fig. SI5). In AaHase both subunits roughly present similar contributions in amplitude, but points toward opposite directions, which results in a low total dipole moment with a fluctuating orientation for the whole enzyme. On the contrary, in DfHase the small subunit has a significantly higher value than the large one and both dipole moments point toward similar directions, thus leading to a strong and stable cumulated dipole moment. As seen from the root-mean-square fluctuation (RMSF) values (Fig. SI6), the large subunit structure fluctuates more than the small one in both proteins. As a consequence, since the weight of the large subunit in the AaHase dipole is higher than in DfHase, the large subunit residues' fluctuations induce large variations of the total dipole moment orientation in the former enzyme.

Although the results displayed in Fig. 3 provide a convincing rationale to the experimental observations, it has to be pointed out that the simulations were carried out without the presence of the AaHase transmembrane helix. Previous work showed that Dodecylmaltoside (DDM) surrounding the trans-membrane helix promotes a high proportion of DET on hydrophilic surfaces, but lessens the DET on hydrophobic SAM.[12] Ciaccafava et al. suggested that the DDM on the hydrophobic trans-membrane helix induces a hydrophilic environment near the distal FeS cluster, thus impairing the interaction with hydrophobic surfaces. In addition, the trans-membrane helix is supposed to adopt different conformations in solution, modulating the orientation of the enzyme as well as the exposition of the distal FeS cluster. Since the helix has a +3 net charge with an almost uniform residue distribution, it is unlikely that its dipole will significantly perturb the overall dipole moment. Here we attempt to address the helix influence on the dipole moment by a simple approach: we used the recently published *E.coli*-cytochrome structure (4GD3)[31] as a template, which led to a homology model of the full length AaHase (Fig.4a). In addition, two different helix conformations were generated using the sculpting module implemented in pymol.[32] In the first one, the helix is oriented toward the large subunit (Fig.4b) while in the other it is oriented toward the small subunit (Fig.4C). The resulting total dipole moments shown in cyan in Fig. 4 confirm that the presence of the helix does not significantly alter its direction. Although the helix in the 4GD3 structure is close to the distal FeS cluster, a 20 residues long unstructured region connects the soluble domain to the helix. This flexible loop likely enables the helix to move freely in solution, preventing steric hindrance between the distal FeS cluster and the surface, and permitting DET with the electrodes as observed by Ciaccafava et al.[12]

## Conclusion

In summary, after performing cyclic voltammetry experiments for AaHase and DfHase immobilized on various functionalized electrodes, we used homology modeling coupled with long timescale MD simulations to assess internal motion in these enzymes. The simulations provide an explanation for the versatility of the AaHase/electrodes interaction: we compared the protein dipole moments and found much weaker values coupled with significant directional fluctuations in AaHase compared to DfHase (Fig.3), which concur with the higher RMSF of the large AaHase subunit with respect to DfHase, and the fact that in DfHase, the (more stable) small subunit contributes much more to the total dipole moment than the (less stable) large subunit. Introducing the trans-membrane helix for AaHase did not change our results (Fig. 4). These data permit to produce a model for a versatile AaHase-electrode interaction. In solution, AaHase adopts different conformations depending on its structural fluctuations, thus leading to various dipole orientations (See Fig. 3c). Since there is no preferential dipole moment direction, the charge of the electrode selects, among the available dipole configurations, the most adapted one, while the other conformations cannot bind the electrode in a DET-compatible orientation (Fig.5). The helix only marginally influences the relative weight of the different dipole moment populations but does not significantly change the general adsorption preference. Further works will address the interaction of AaHase and other $O_2$-tolerant MBHs with the electrodes in more details. In particular, we intend to perform calculations on the MBH from *E. Coli*, which is known to form a dimer of heterodimers,[16, 31] and investigate how this configuration affects the system's dipole moment and its binding onto electrodes. We will also investigate how the protein/electrode interaction impacts the enzyme's conformation and flexibility and therefore its biological function. Finally, another immediate goal is to improve biofuel cell design to better accommodate the AaHase characteristics and, eventually, optimize the efficiency of the overall system.

## Acknowledgements

The authors thank the Programme Interdisciplinaire Energie CNRS and the ANR Bioénergies for financial support (Grant ANR-10-BIOE-003). This work was further supported by the «Initiative d'Excellence» program from the French State (Grant «DYNAMO», ANR-11-LABX-0011).

## Notes and references

[a] Laboratoire de Biochimie Théorique, UPR 9080 CNRS Institut de Biologie Physico-Chimique, 13 rue Pierre et Marie Curie, 75005 Paris, France

[b] Bioénergétique et Ingénierie des Protéines, Institut de Microbiologie de la Méditerranée-CNRS-Aix Marseille University, 31 Chemin Joseph Aiguier, 13402 Marseille Cedex 20, France.

Electronic Supplementary Information (ESI) available: [details of any supplementary information available should be included here]. See DOI: 10.1039/b000000x/

1. M. W. W. Adams, L. E. Mortenson and J. S. Chen, *Biochim. Biophys. Acta*, 1980, **594**, 105-176.
2. P. M. Vignais and B. Billoud, *Chemical Reviews*, 2007, **107**, 4206-4272.
3. E. Lojou, *Electrochim. Acta*, 2011, **56**, 10385-10397.
4. A. Ciaccafava, A. De Poulpiquet, V. Techer, M. T. Giudici-Orticoni, S. Tingry, C. Innocent and E. Lojou, *Electrochemistry Communications*, 2012, **23**, 25-28.
5. L. Xu and F. A. Armstrong, *Energy & Environmental Science*, 2013, **6**, 2166-2171.
6. D. H. Kim and M. S. Kim, *Bioresour. Technol.*, 2011, **102**, 8423-8431.
7. M. Brugna-Guiral, P. Tron, W. Nitschke, K. O. Stetter, B. Burlat, B. Guigliarelli, M. Bruschi and M. T. Giudici-Orticoni, *Extremophiles*, 2003, **7**, 145-157.
8. J. C. Fontecilla-Camps, A. Volbeda, C. Cavazza and Y. Nicolet, *Chem Rev*, 2007, **107**, 4273-4303.
9. X. J. Luo, M. Brugna, P. Tron-Infossi, M. T. Giudici-Orticoni and E. Lojou, *Journal of Biological Inorganic Chemistry*, 2009, **14**, 1275-1288.
10. E. Lojou, X. Luo, M. Brugna, N. Candoni, S. Dementin and M. T. Giudici-Orticoni, *Journal of biological inorganic chemistry : JBIC : a publication of the Society of Biological Inorganic Chemistry*, 2008, **13**, 1157-1167.

11. A. Ciaccafava, P. Infossi, M. Ilbert, M. Guiral, S. Lecomte, M. T. Giudici-Orticoni and E. Lojou, *Angew Chem Int Ed Engl*, 2012, **51**, 953-956.
12. A. Ciaccafava, A. De Poulpiquet, P. Infossi, S. Robert, R. Gadiou, M. T. Giudici-Orticoni, S. Lecomte and E. Lojou, *Electrochim. Acta*, 2012, **82**, 115-125.
13. J. Fritsch, S. Loscher, O. Sanganas, E. Siebert, I. Zebger, M. Stein, M. Ludwig, A. L. De Lacey, H. Dau, B. Friedrich, O. Lenz and M. Haumann, *Biochemistry*, 2011, **50**, 5858-5869.
14. Y. Shomura, K. S. Yoon, H. Nishihara and Y. Higuchi, *Nature*, 2011, **479**, 253-U143.
15. A. Volbeda, M. H. Charon, C. Piras, E. C. Hatchikian, M. Frey and J. C. Fontecilla-Camps, *Nature*, 1995, **373**, 580-587.
16. A. Volbeda, P. Amara, C. Darnault, J. M. Mouesca, A. Parkin, M. M. Roessler, F. A. Armstrong and J. C. Fontecilla-Camps, *Proceedings of the National Academy of Sciences of the United States of America*, 2012, **109**, 5305-5310.
17. R. M. Evans, A. Parkin, M. M. Roessler, B. J. Murphy, H. Adamson, M. J. Lukey, F. Sargent, A. Volbeda, J. C. Fontecilla-Camps and F. A. Armstrong, *J. Am. Chem. Soc.*, 2013, **135**, 2694-2707.
18. J. M. Mouesca, J. C. Fontecilla-Camps and P. Amara, *Angew Chem Int Ed Engl*, 2013, **52**, 2002-2006.
19. J. Fritsch, P. Scheerer, S. Frielingsdorf, S. Kroschinsky, B. Friedrich, O. Lenz and C. M. Spahn, *Nature*, 2011, **479**, 249-252.
20. T. Goris, A. F. Wait, M. Saggu, J. Fritsch, N. Heidary, M. Stein, I. Zebger, F. Lendzian, F. A. Armstrong, B. Friedrich and O. Lenz, *Nat Chem Biol*, 2011, **7**, 310-318.
21. A. Fiser, R. K. Do and A. Sali, *Protein science : a publication of the Protein Society*, 2000, **9**, 1753-1773.
22. A. Fiser and A. Sali, *Methods Enzymol.*, 2003, **374**, 461-491.
23. B. Hess, F. Kutzner, D. Van der Spoel and E. Lindahl, *J. Chem. Theory Comput.*, 2008, **4**, 435-447.
24. T. Utesch, D. Millo, M. A. Castro, P. Hildebrandt, I. Zebger and M. A. Mroginski, *Langmuir*, 2013, **29**, 673-682.
25. O. Rudiger, C. Gutierrez-Sanchez, D. Olea, I. A. C. Pereira, M. Velez, V. M. Fernandez and A. L. De Lacey, *Electroanalysis*, 2010, **22**, 776-783.
26. N. Yahata, T. Saitoh, Y. Takayama, K. Ozawa, H. Ogata, Y. Higuchi and H. Akutsu, *Biochemistry*, 2006, **45**, 1653-1662.
27. T. Lojou and P. Bianco, *Langmuir*, 2004, **20**, 748-755.
28. P. Bianco, J. Haladjian and S. Giannandreaderocles, *Electroanalysis*, 1994, **6**, 67-74.
29. F. A. Armstrong, P. A. Cox, H. A. O. Hill, V. J. Lowe and B. N. Oliver, *J. Electroanal. Chem.*, 1987, **217**, 331-366.
30. D. Millo, M. E. Pandelia, T. Utesch, N. Wisitruangsakul, M. A. Mroginski, W. Lubitz, P. Hildebrandt and I. Zebger, *Journal of Physical Chemistry B*, 2009, **113**, 15344-15351.
31. A. Volbeda, C. Darnault, A. Parkin, F. Sargent, F. A. Armstrong and J. C. Fontecilla-Camps, *Structure*, 2013, **21**, 184-190.
32. Schrodinger, LLC, 2010.

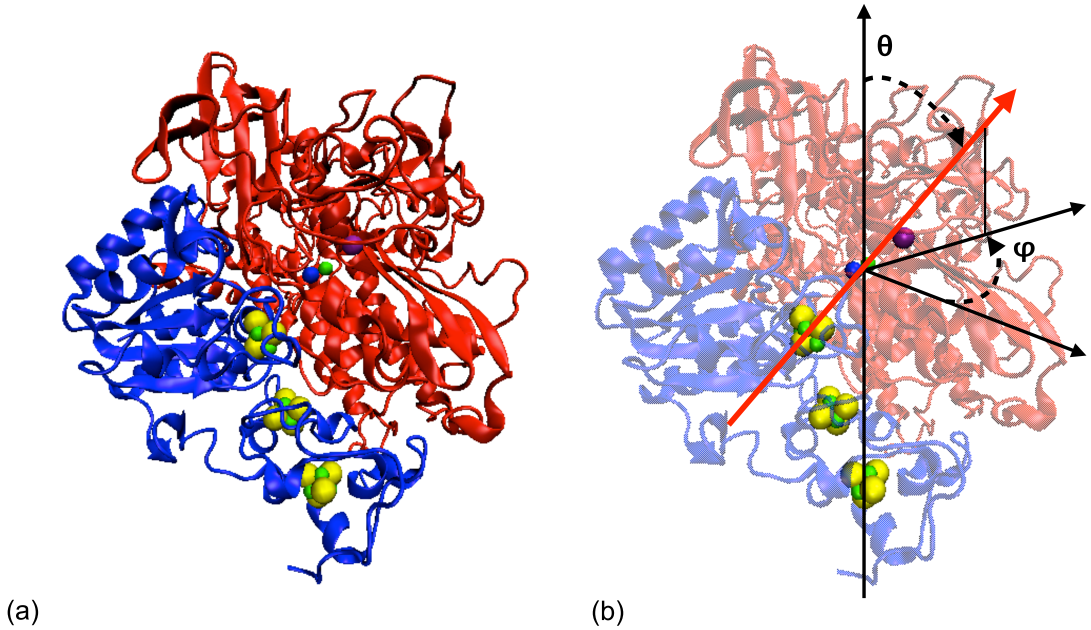

**Figure 1.** (a) Structure of AaHase with the large and small subunits in red and blue respectively. The active [NiFe] site, the $Mg^{2+}$ ion and the FeS clusters are represented as Van der Waals spheres. (b) Reference system for the Hase dipole moment (red arrow) orientation via the θ and φ angles.

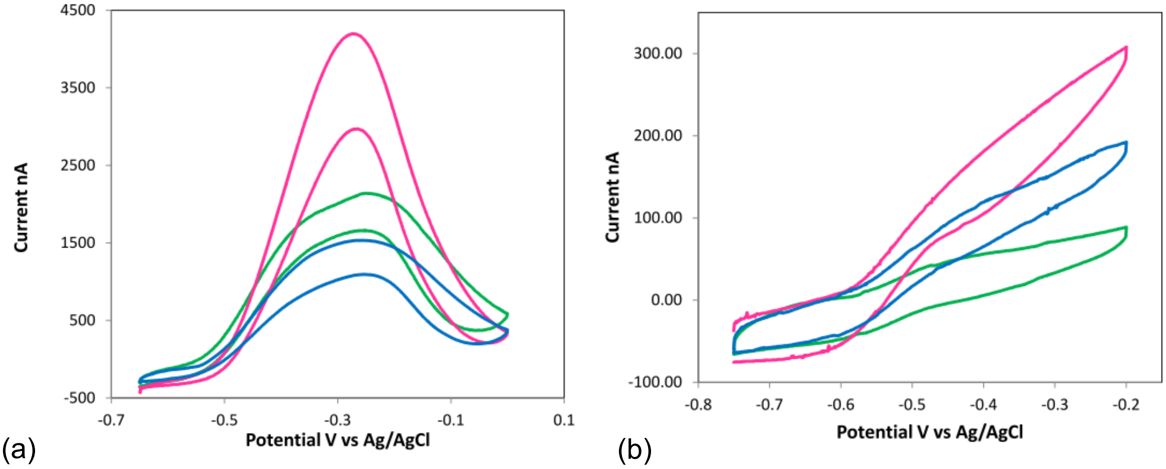

(a) (b)

**Figure 2.** Voltammetric hydrogen oxidation by Aa (a) and Df (b) Hases immobilized on a bare graphite electrode (blue), or modified by positively charged poly(L-lysine) (red) or negatively charged poly(L-glutamate) (green). Hepes Buffer 50 mM, pH 7.2, 5 mV.s$^{-1}$. Temperature was 25°C and 60°C for Df and Aa Hases respectively.

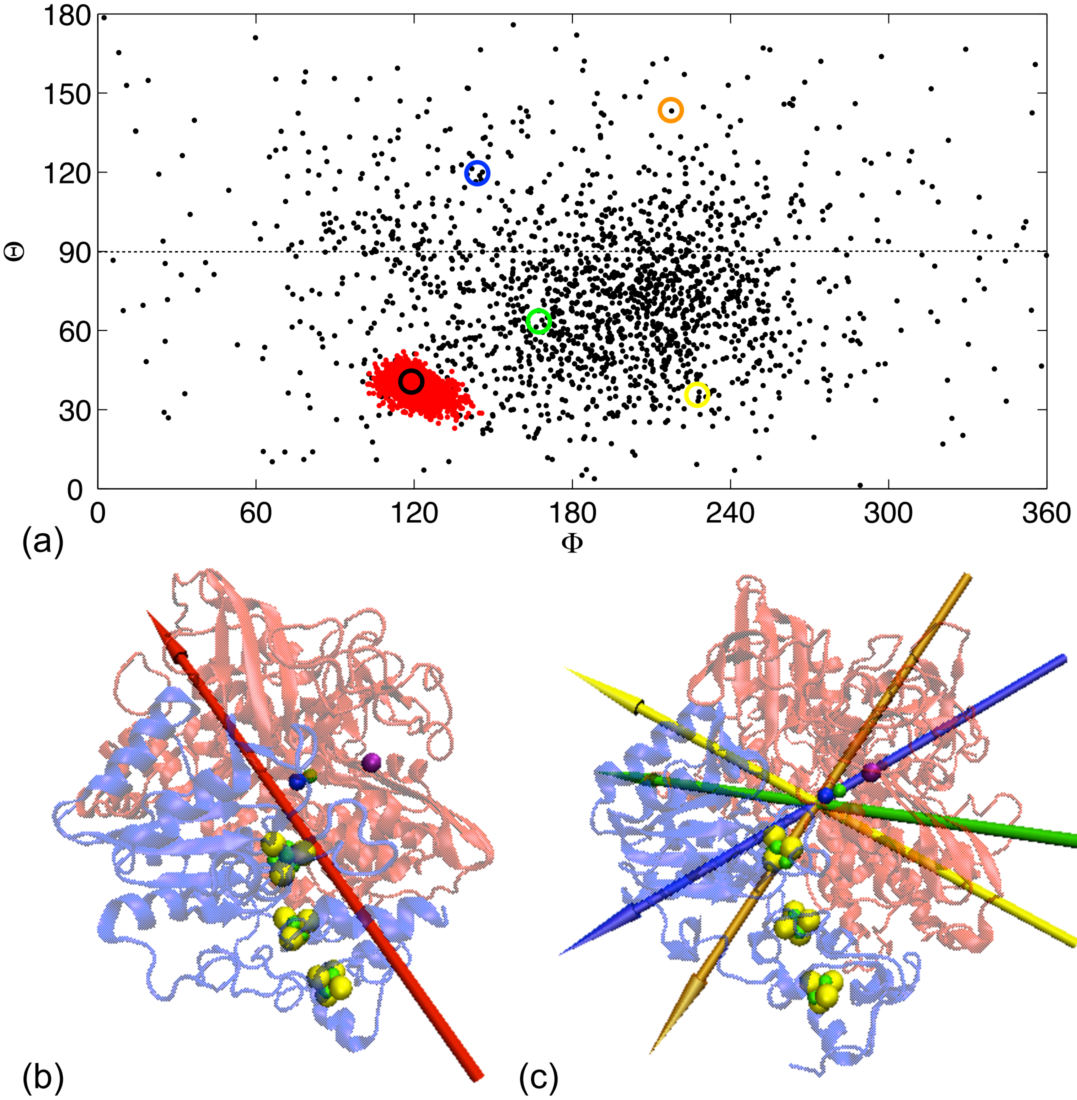

**Figure 3.** (a) Distribution of the dipole moment orientation during MD trajectories for AaHase (black dots) and DfHase (red dots). (b) Representative snapshot of the dipole moment for DfHase corresponding to the black circle on panel (a). (c) Representative snapshots of the dipole moment for AaHase, corresponding to the blue, green, yellow and orange circles in panel (a).

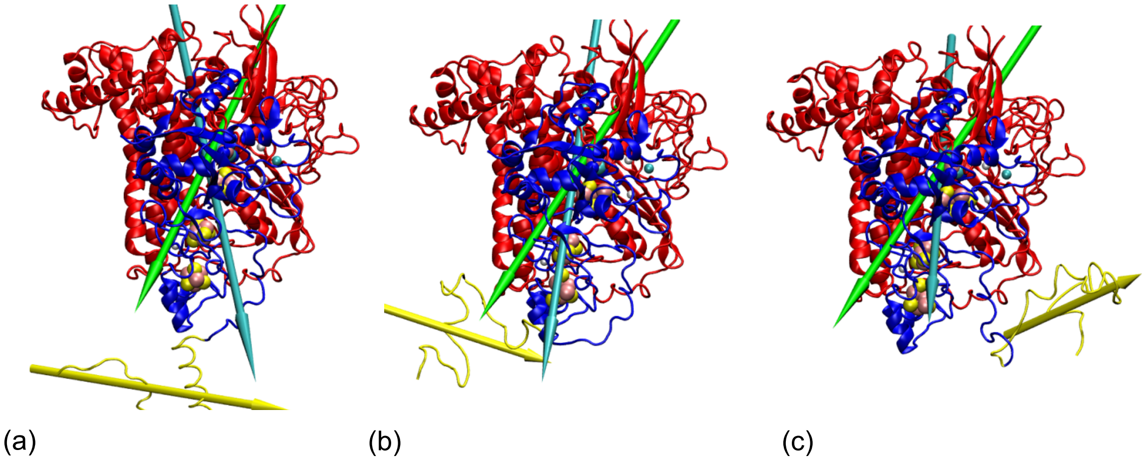
(a) (b) (c)

**Figure 4.** Dipole moment of AaHase as a function of the trans-membrane helix orientation. The arrows represent the dipole moment for the soluble domain (green), the helix (yellow), and the whole protein (cyan). The conformation of the helix has been taken from the homology model (a) and oriented towards the large (b) or small subunit (c).

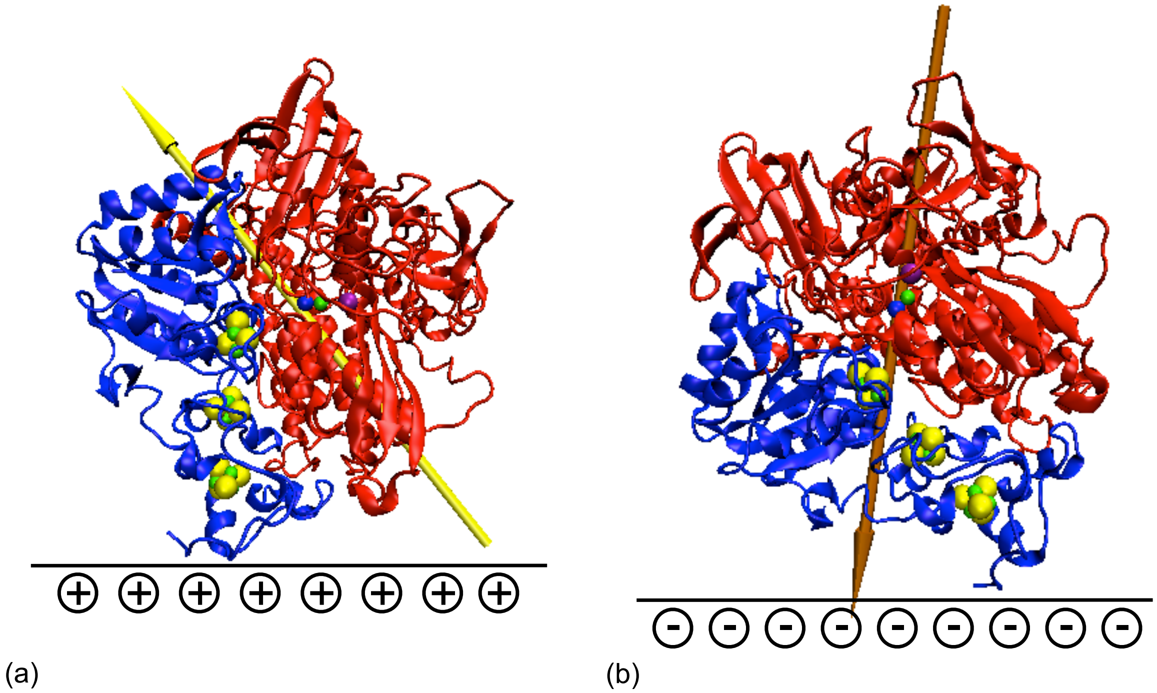

**Figure 5**. Configuration of the AaHase bound to a positive (a) and negative (b) electrode. The proteins have been oriented following their dipole moment and then adjusted to position the distal FeS cluster as close as possible to the surface.

PCCP RSCPublishing

ARTICLE

## Supporting Information

## METHODS

**Starting Structures.** The wild type DfHase crystal structure (PDB-id 1FRF) has been used as starting structure for the DfHase simulation, while comparative homology modeling was used to build the starting structure for AaHase. The amino acid sequences of the two soluble AaHase domains have been taken from the GenBank id AAC06862.1 (small subunit) and AAC06861.1 (large subunit). MODELLER v9.10[1,2] was used to build the starting structure using the following templates: Desulfovibrio desulfuricans (1E3D)[3], Desulfovibrio vulgaris Miyazaki (1WUI)[4], Desulfovibrio gigas (1FRV)[5], Desulfovibrio fructosovorans (1YQW)[6], Hydrogenovibrio marinus (3AYX)[7], Ralstonia eutropha (3RGW)[8] and Allochromatium vinosum (3MYR)[9]. The structures were superimposed using Chimera[10,11] and used as input for MODELLER. Regarding the small subunit, only the residues for the soluble domain (i.e. from P47 to G316), were retained. The metallic centers were obtained from the oxygen tolerant hydrogenase of Hydrogenovibrio marinus[7] and were treated as rigid blocks during the modeling procedure. The loops originating from gaps in the alignment were energy-optimized in order to obtain a refined, energetically favorable structure according to the dope-score of the Modeller v9.10 software. The secondary structure regularity and the degree of steric clashes in the model were evaluated using the MolProbity (http://molprobity.biochem.duke.edu) web server[12] at two different stages namely on the starting model and after the equilibration.

**Metal centre parametrization**. In this paper we attempt to study the hydrogenase enzymes in the oxidation state prior to $H_2$ processing. According to Niu and coworkers[13], the active site has been assumed to be in the Ni-SIa state (total charge of -2) while the FeS clusters were treated as oxidized. Parameters for the [4Fe4S] proximal cluster in DfHase were obtained from[14], while the medial clusters were parametrized according to ref.[15]. Charges for the remaining metallic centers (i.e. active site, the distal and medial clusters and the proximal cluster of AaHase) were obtained through the R.E.D. Server[16] using the RESP-X1 charge model and are reported in Table 1 of this Supplementary Information. To reduce the complexity of the calculations, only the side chains have been retained. The Cβ has been treated as a methyl group and the neutrality has been imposed to these four atoms. The metallic centers were maintained rigid during the simulations through an elastic network (spring force constant 200 kJ) between the metallic atoms and the carbons of the side chains. It is worth stressing that the primary aim of this study was the global characterization of the protein motion that is not supposed to be influenced by the approximations in the parameterization of the metal centers. During the writing of this paper the metallic centers of oxygen-tolerant hydrogenases were more accurately parametrized[17], providing a starting point for future studies. Among the possible states of the AaHase proximal cluster (reduced, oxidized and superoxidized), the oxidized state has been used for two reasons. The first is in order to assign the same charge (-2) in both simulations. The second is that deriving the parameters is less ambiguous because in this state the N of $C26^S$ is protonated.

**System parametrization.** The proteins were solvated in a cubic box of water and afterwards $Na^+$ and $Cl^-$ ions were added at a concentration of 0.150 M. The systems were represented using CHARM27 with CMAP corrections[18] and the standard TIP3P water model as implemented in the GROMACS software[19] was used. The protonation state has been chosen according to the most probable one at pH 7.

**Simulation set-up.** The two systems were simulated using GROMACS 4.5.3[20]. The systems were initially energy minimized for 2000 steps, then equilibrated by simulating for 1 ns in the NVT ensemble and subsequently for 1 ns in the NPT ensemble, prior to starting production runs of 2 microsecond duration. The temperature of protein and solvent (water and ions) was separately regulated using the Velocity Rescaling[21] method with a reference temperature of 300K and a coupling constant of 1ps for the two groups. The Parinello-Rahman[22,23] algorithm was adopted to maintain the pressure at 1 atm. The SETTLE[24] algorithm was employed to maintain the water rigidity and LINCS[25,26] to constrain the covalent bonds involving hydrogen atoms. The two optimized and relaxed systems were simulated for 2 microseconds, with a 2.0 fs time step, in periodic boundary conditions. Van der Waals interactions were switched off between 1.0 to 1.2 nm, updating the neighbor pair lists every 10 steps while the long range electrostatic interactions were evaluated through the particle-mesh Ewald method[27] using a cut-off of 1.2 nm.

**Analysis.** Unless otherwise stated, the trajectories were skipped every 5 ps and analyzed with GROMACS 4.5.5 analysis tools. All the plots were depicted through Matplotlib[28], while structures have been depicted using VMD 1.9.1[29] and Chimera[11]. Since the RMSD reaches a stable plateau within 200 ns, the analysis has been carried out on the last 1.8 μs, considering the initial 200 ns as equilibration period.

The electrostatic potentials have been calculated using the conformation at time 2 μs using the APBS 1.3 software[30] assigning the charges used in the simulation.

The dipole moment has been calculated through the Dipole Watcher VMD plugin and afterwards the vector components have been used to obtain the θ and φ angles. θ defines the dipole moment inclination with respect to the Z axis, which goes through the distal FeS cluster and the [NiFe] active site (see Fig. 1b), while the φ angle depends on the dipole moment orientation with respect to [NiFe]-$Mg^{2+}$ ion axis.

**Modeling of the AaHase trans-membrane helix.** The recently published E.coli-cytochrome structure (4GD3)[31] has been used as template to build a homology model of the full length AaHase (Fig.4a). To assess the influence of the trans-membrane helix on the overall dipole moment, two additional helix conformations have been generated using the sculpting module implemented in Pymol. In the former conformation, the helix is oriented toward the large subunit (Fig.4b) while in the latter it is oriented toward the small subunit (Fig.4c).

**Quality assessement.** The quality of the homology model has been assessed through MolProbity[12]. This software provides a score resuming the model quality in terms of steric clashes and deviation of the backbone dihedral angles from any of the Ramachandran regions describing α-helices and ß-sheets. The analysis performed on the starting model displays that 96.6% of the residues belong to the favored region and 99.5% are in the allowed region; at the end of the thermalization (i.e. 0 ns) several residues on the border between helices and loop became unstructured so the percentage of the residues belonging to favored and allowed regions slightly decreased to 92.9% and 98.5% respectively. The residues of the long loop ranging from Tyr142 to Lys161 from the large subunit retained the unstructured conformation and compose, together with the other loops, the residues in the forbidden region.

The final structure of AaHase can be downloaded as a pdb file at the following address: http://www.lojou.fr/biopac/?page=./common/bibliotheque.php&display=0

**References:**

[1] A. Fiser, A. Sali, in Methods Enzymol., Elsevier, **2003**, pp. 461–491.

[2] A. Fiser, R. K. Do, A. Sali, Protein Sci. Publ. Protein Soc. **2000**, 9, 1753–1773.

[3] P. M. Matias, C. M. Soares, L. M. Saraiva, R. Coelho, J. Morais, J. Le Gall, M. A. Carrondo, J. Biol. Inorg. Chem. JBIC Publ. Soc. Biol. Inorg. Chem. **2001**, 6, 63–81.

[4] H. Ogata, S. Hirota, A. Nakahara, H. Komori, N. Shibata, T. Kato, K. Kano, Y. Higuchi, Structure **2005**, 13, 1635–1642.

[5] A. Volbeda, M. H. Charon, C. Piras, E. C. Hatchikian, M. Frey, J. C. Fontecilla-Camps, Nature **1995**, 373, 580–587.

[6] A. Volbeda, L. Martin, C. Cavazza, M. Matho, B. Faber, W. Roseboom, S. Albracht, E. Garcin, M. Rousset, J. Fontecilla-Camps, JBIC J. Biol. Inorg. Chem. **2005**, 10, 239–249.

[7] Y. Shomura, K.-S. S. Yoon, H. Nishihara, Y. Higuchi, Nature **2011**, 479, 253–256.

[8] J. Fritsch, P. Scheerer, S. Frielingsdorf, S. Kroschinsky, B. Friedrich, O. Lenz, C. M. Spahn, Nature **2011**, 479, 249–252.

[9] H. Ogata, P. Kellers, W. Lubitz, J. Mol. Biol. **2010**, 402, 428–444.

[10] G. S. Couch, D. K. Hendrix, T. E. Ferrin, Nucleic Acids Res. **2006**, 34, e29.

[11] E. F. Pettersen, T. D. Goddard, C. C. Huang, G. S. Couch, D. M. Greenblatt, E. C. Meng, T. E. Ferrin, J. Comput. Chem. **2004**, 25, 1605–1612.

[12] I. W. Davis, A. Leaver-Fay, V. B. Chen, J. N. Block, G. J. Kapral, X. Wang, L. W. Murray, W. B. Arendall, J. Snoeyink, J. S. Richardson, et al., Nucleic Acids Res. **2007**, 35, W375–W383.

[13] S. Niu, L. M. Thomson, M. B. Hall, J. Am. Chem. Soc. **1999**, 121, 4000–4007.

[14] C. H. Chang, K. Kim, J. Chem. Theory Comput. **2009**, 5, 1137–1145.

[15] M. Meuwly, M. Karplus, Faraday Discuss. **2003**, 124.

[16] F.-Y. Y. Dupradeau, A. Pigache, T. Zaffran, C. Savineau, R. Lelong, N. Grivel, D. Lelong, W. Rosanski, P. Cieplak, Phys. Chem. Chem. Phys. PCCP **2010**, 12, 7821–7839.

[17] D. M. A. Smith, Y. Xiong, T. P. Straatsma, K. M. Rosso, T. C. Squier, J. Chem. Theory Comput. **2012**, 8, 2103–2114.

[18] A. D. MacKerell, M. Feig, C. L. Brooks, J. Am. Chem. Soc. **2003**, 126, 698–699.

[19] P. Bjelkmar, P. Larsson, M. A. Cuendet, B. Hess, E. Lindahl, J. Chem. Theory Comput. **2010**, 6, 459–466.

[20] B. Hess, C. Kutzner, D. van der Spoel, E. Lindahl, J. Chem. Theory Comput. **2008**, 4, 435–447.

[21] G. Bussi, M. Parrinello, Phys. Rev. E **2007**, 75, 056707+.

[22] S. Nosé, M. L. Klein, Mol. Phys. **1983**, 50, 1055–1076.

[23] M. Parrinello, A. Rahman, J. Appl. Phys. **1981**, 52, 7182–7190.

[24] S. Miyamoto, P. A. Kollman, J Comput Chem **1992**, 13, 952–962.

[25] B. Hess, J. Chem. Theory Comput. **2007**, 4, 116–122.

[26] B. Hess, H. Bekker, H. J. C. Berendsen, J. G. E. M. Fraaije, J Comput Chem **1997**, 18, 1463–1472.

[27] U. Essmann, L. Perera, M. L. Berkowitz, T. Darden, H. Lee, L. G. Pedersen, J. Chem. Phys. **1995**, 103, 8577–8593.

[28] J. D. Hunter, Comput. Sci. Eng. **2007**, 9, 90–95.

[29] W. Humphrey, A. Dalke, K. Schulten, J. Mol. Graph. **1996**, 14.

[30] N. A. Baker, D. Sept, S. Joseph, M. J. Holst, J. A. McCammon, Proc. Natl. Acad. Sci. **2001**, 98, 10037–10041.

[31] A. Volbeda, C. Darnault, A. Parkin, F. Sargent, F. A. Armstrong, J. C. Fontecilla-Camps, Struct. Lond. Engl. 1993 **2013**, 21, 184–190.

[32] X. Luo, M. Brugna, P. Tron-Infossi, M. T. T. Giudici-Orticoni, E. Lojou, J. Biol. Inorg. Chem. JBIC Publ. Soc. Biol. Inorg. Chem. **2009**, 14, 1275–1288.

## FIGURE LEGENDS

**Supplementary figure 1.** Parameterized metallic centers. The atomic name is reported only for the inorganic parts in order to allow the comparison with table 1 of Supplementary Information. Panel A represents the active site, panel B the proximal FeS cluster while panel C reports the distal FeS cluster.

**Supplementary figure 2.** Surface characteristics for AaHase (left) and DfHase (right) from six different views (panel I to VI). The top rows recall the orientation of the protein, the middle one shows the electrostatic potential (at 2 kT) as identified in Table 2 of Supplementary Information.

**Supplementary figure 3.** Dipole moment strength as a function of time for AaHase (black line) and DfHase (red line).

**Supplementary figure 4.** Dipole moment strength as a function of time for the small (black line) and large (red line) subunit for AaHase (Panel A) and DfHase (Panel B).

**Supplementary figure 5.** Angle between the dipole moment contributions of the large and small subunits as a function of time in AaHase (black line) and DfHAse (red line)

**Supplementary figure 6.** RMSF for each residue of the small (Panel A) and large (Panel B) subunit for AaHAse (black) and DfHase (red). The residues have been aligned based on their similarity. The Cysteines coordinating the active site, proximal, medial and distal cluster have been denoted as AS, P, M and D respectively. The blue rectangle represents the long loop. The horizontal line indicates the threshold value chosen for the selection of the fluctuating residues (0.1 nm).

| Center | Atom | Charge |
|---|---|---|
| Active Site | Ni | 0.40 |
| | Fe | 0.23 |
| | C | 0.22 |
| | O | −0.294 |
| | C | 0.11 |
| | N | −0.61 |
| Cys65/610 | CB | −0.03 |
| | HB1 | 0.08 |
| | HB2 | 0.08 |
| | SG | −0.39 |
| Cys62/607t | CB | −0.05 |
| | HB1 | 0.051 |
| | HB2 | 0.051 |
| | SG | −0.57 |
| 4Fe3S Proximal FeS cluster | Fe1 | 0.4349 |
| | Fe2 | 0.3710 |
| | Fe3 | 0.5092 |
| | Fe4 | 0.3965 |
| | S1 | −0.3661 |
| | S2 | −0.3728 |
| | S3 | −0.3076 |
| Cys59 | CB | −0.0751 |
| | HB1 | 0.065 |
| | HB2 | 0.065 |
| | SG | −0.5387 |
| Cys61 | CB | −0.1877 |
| | HB1 | 0.126 |
| | HB2 | 0.126 |
| | SG | −0.2863 |
| Cys62 | CB | −0.0884 |
| | HB1 | 0.0693 |
| | HB2 | 0.0693 |
| | SG | −0.6067 |
| Cys191 | CB | 0.0656 |
| | HB1 | −0.0044 |
| | HB2 | −0.0044 |
| | SG | −0.5784 |
| | CB | −0.0247 |

| | | |
|---|---|---|
| **Cys162** | **HB1** | **0.0448** |
| | **HB2** | **0.0448** |
| | **SG** | **-0.5055** |
| **Distal FeS cluster** | **Fe1** | **0.0505** |
| | **Fe2** | **0.3725** |
| | **Fe3** | **0.3102** |
| | **Fe4** | **0.3965** |
| | **S1** | **-0.3057** |
| | **S2** | **-0.2484** |
| | **S3** | **-0.2352** |
| | **S4** | **-0.2266** |
| **Cys232** | **CB** | **-0.0455** |
| | **HB1** | **0.0645** |
| | **HB2** | **0.0645** |
| | **SG** | **-0.5437** |
| **Cys257** | **CB** | **0.0187** |
| | **HB1** | **0.0453** |
| | **HB2** | **0.0453** |
| | **SG** | **-0.5820** |
| **Cys263** | **CB** | **-0.0176** |
| | **HB1** | **0.056** |
| | **HB2** | **0.056** |
| | **SG** | **-0.5302** |
| **Hys229** | **CB** | **-0.1479** |
| | **HB1** | **0.099** |
| | **HB2** | **0.099** |
| | **CG** | **0.0620** |
| | **ND1** | **-0.0286** |
| | **CE1** | **-0.0292** |
| | **HE1** | **0.1507** |
| | **NE2** | **-0.2535** |
| | **HE2** | **0.3341** |
| | **CD2** | **-0.1953** |
| | **HD2** | **0.1646** |

**Table 1: Charges used in this work**: The atom names of the amino acids follow the CHARMM convention, while for the inorganic parts the name agrees with the Fig.SI1 of Supporting Information.

| | Lobe | L | S |
|---|---|---|---|
| AaHase | A | D7 E19 D31 D410 E411 E580 E581 D585 E596 | E96 E99 E125 D126 E139 E143 |
| | B | D116 E122 D127 E140 E147 D151 D195 E205 | E85 E108 |
| | C | D219 E223 D252 D253 E261 E267 D268 E275 D278 D454 E455 | |
| | D | D82 E359 E362 D512 E519 D522 | D245 D248 D249 |
| | **E** | **K160 K161 K164 R171 K175 K176 K178 K179** | |
| | **F** | | **K187 R210 K221** |
| | **G** | | **K178 K181** |
| | **H** | **K531 K550** | **K167 K260 R308** |
| | **I** | **K330 K331 K351 K358 K444** | |
| DfHase | A | D298 D299 E445 D453 E461 | E135 D252 D255 E262 D170 E171 E181 D185 E194 E197 E250 D203 E262 |
| | B | D19 D363 D364 D366 | E54 E62 E65 D68 E96 |
| | C | D149 E264 D405 | |
| | D | K135 K140 K143 K189 | |
| | E | K245 K256 K444 K452 | |

**Table 2: Residues lining the electrostatic lobes in Fig.SI2 of Supporting Information.**

Figure SI1

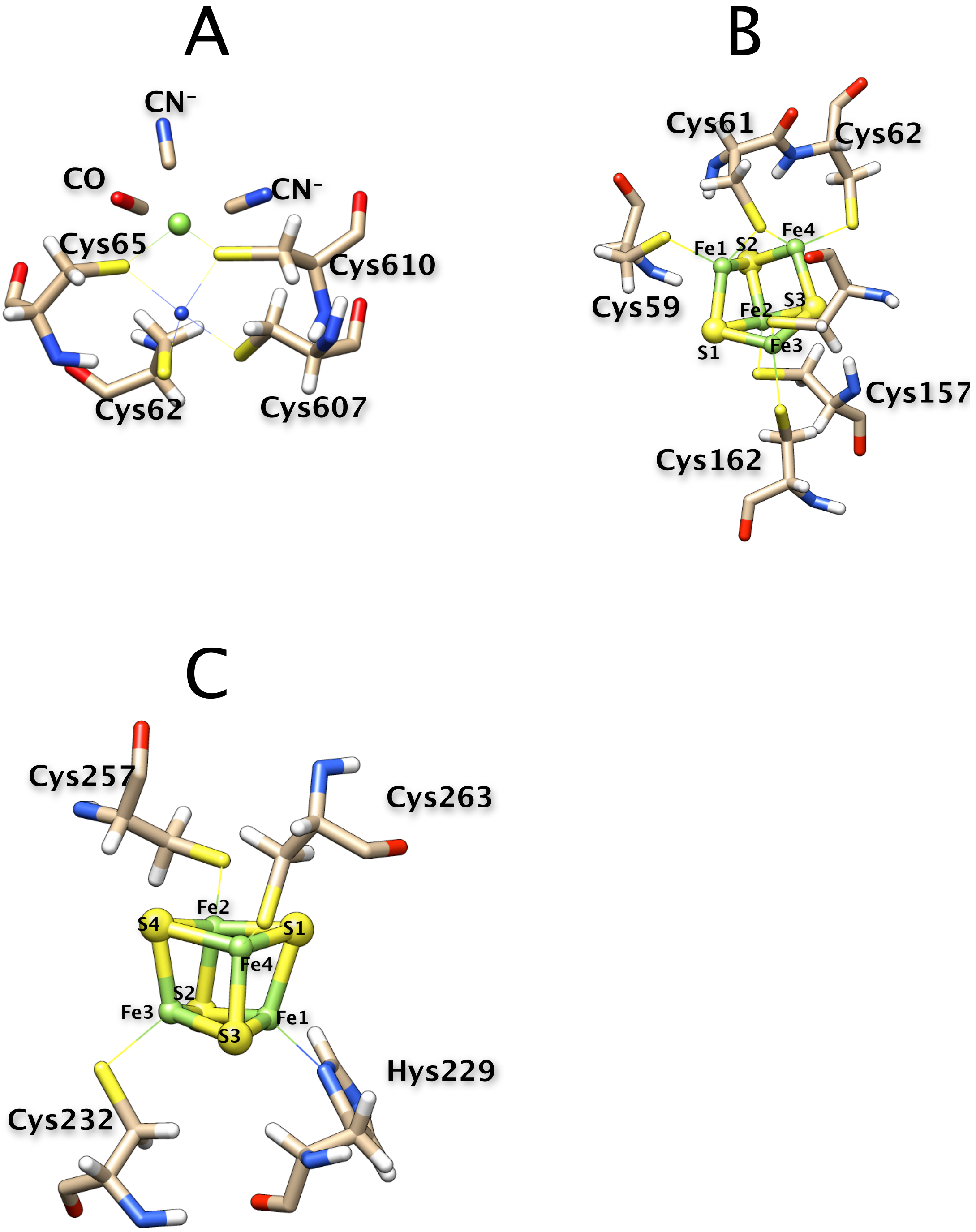
A
CN⁻
CO
CN⁻
Cys65
Cys610
Cys62
Cys607
B
Cys61
Cys62
Fe1
S2
Fe4
Cys59
Fe2
S3
S1
Fe3
Cys157
Cys162
C
Cys257
Cys263
Fe2
S4
S1
Fe4
S2
Fe3
Fe1
S3
Hys229
Cys232

Figure SI2

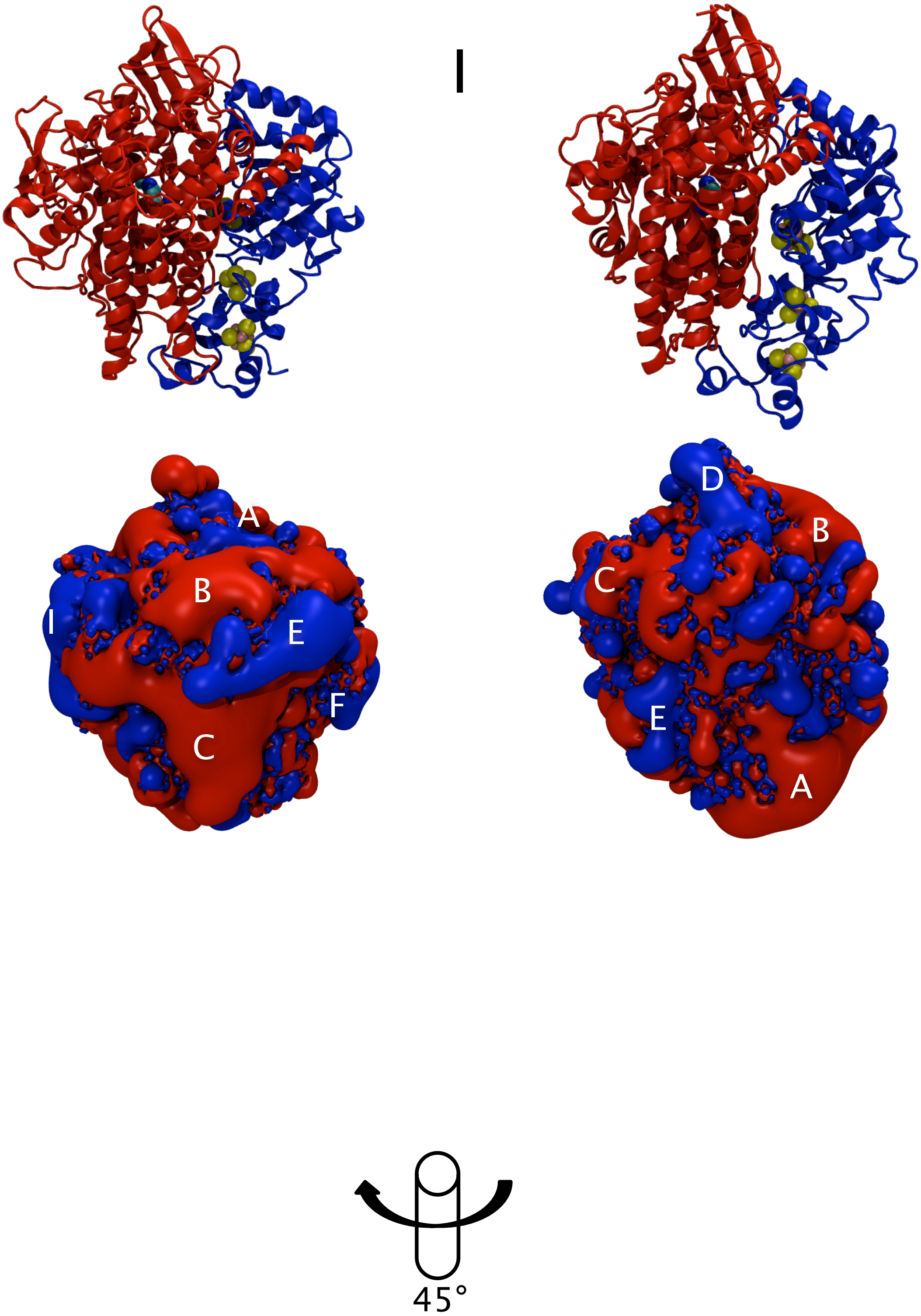
I
A
B
I
E
F
C
D
B
C
E
A
45°

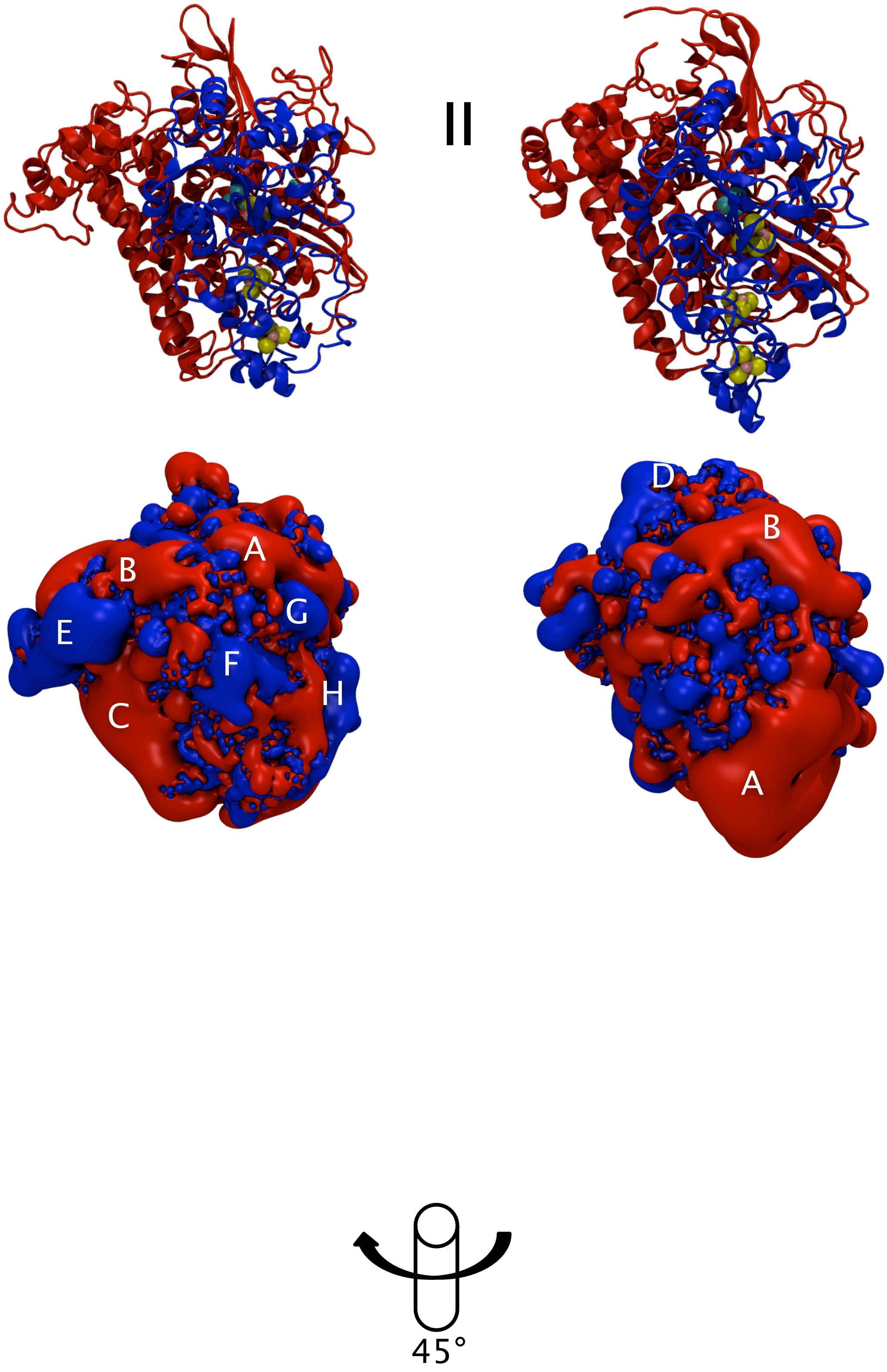
A
B
G
E
F
H
C
D
B
A
45°

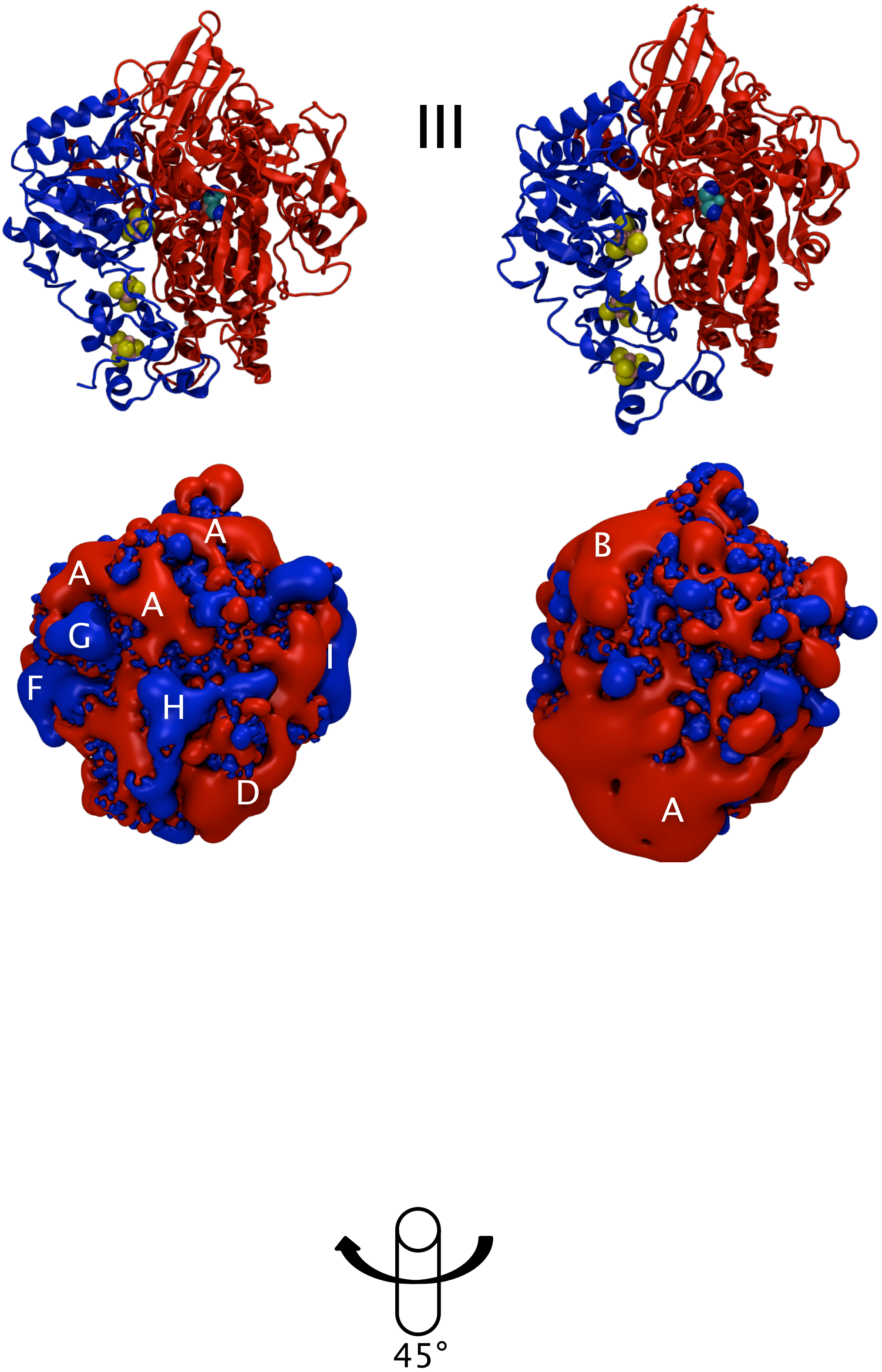
III
A
A
A
G
F
H
I
D
B
A
45°

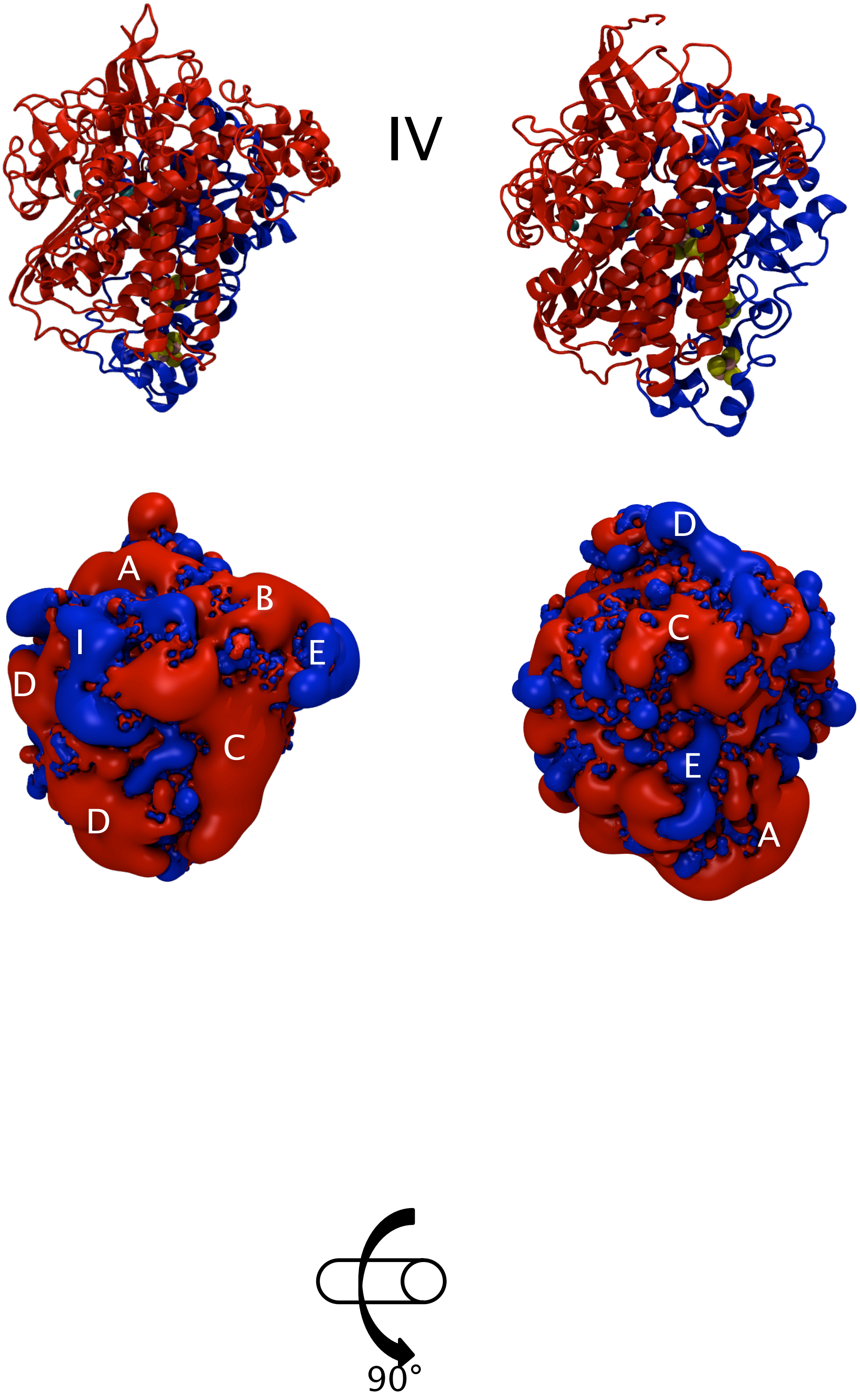
IV
A
B
I
E
D
C
D
D
C
E
A
90°

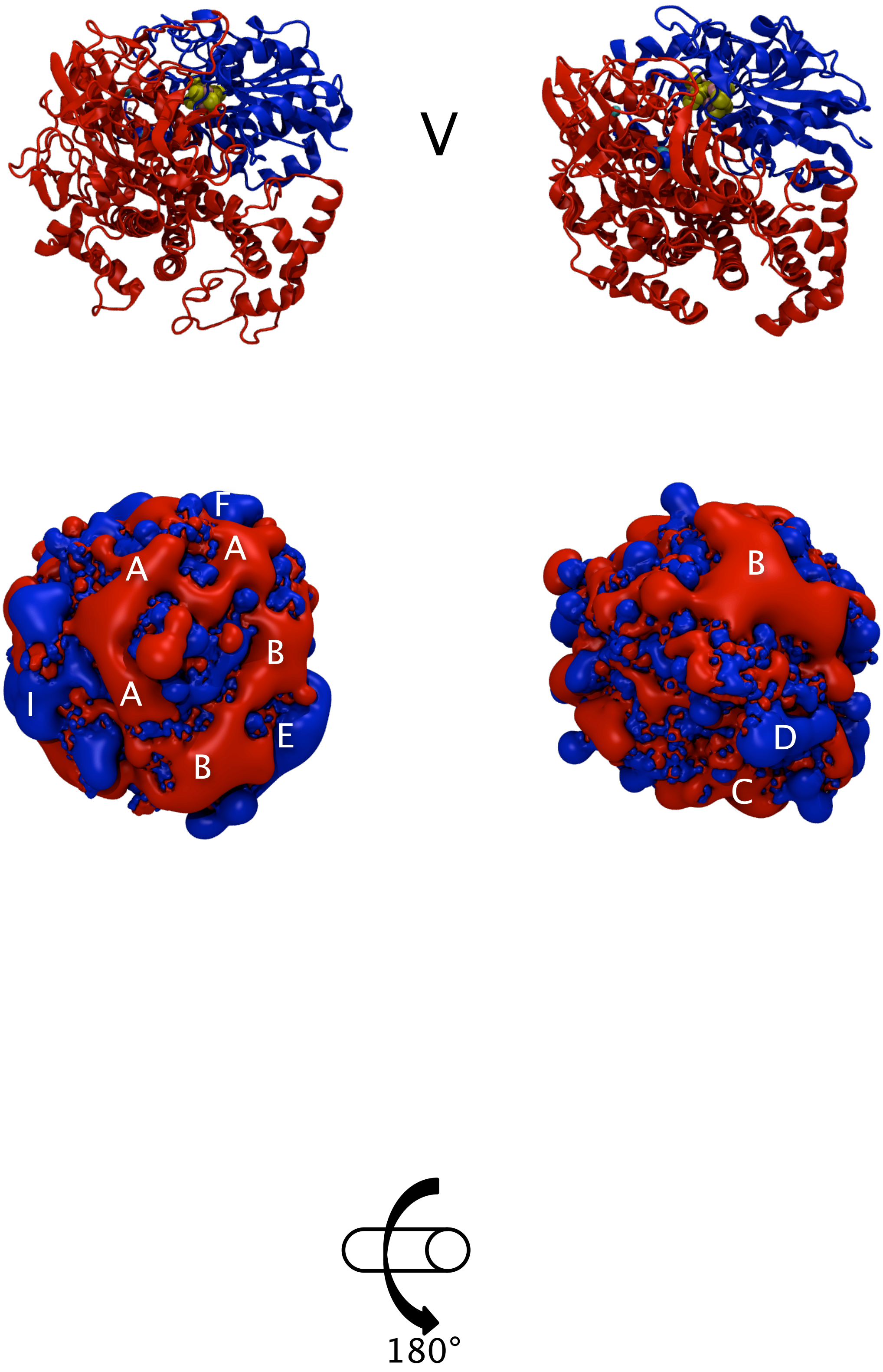
V
F
A
A
B
A
I
E
B
B
D
C
180°

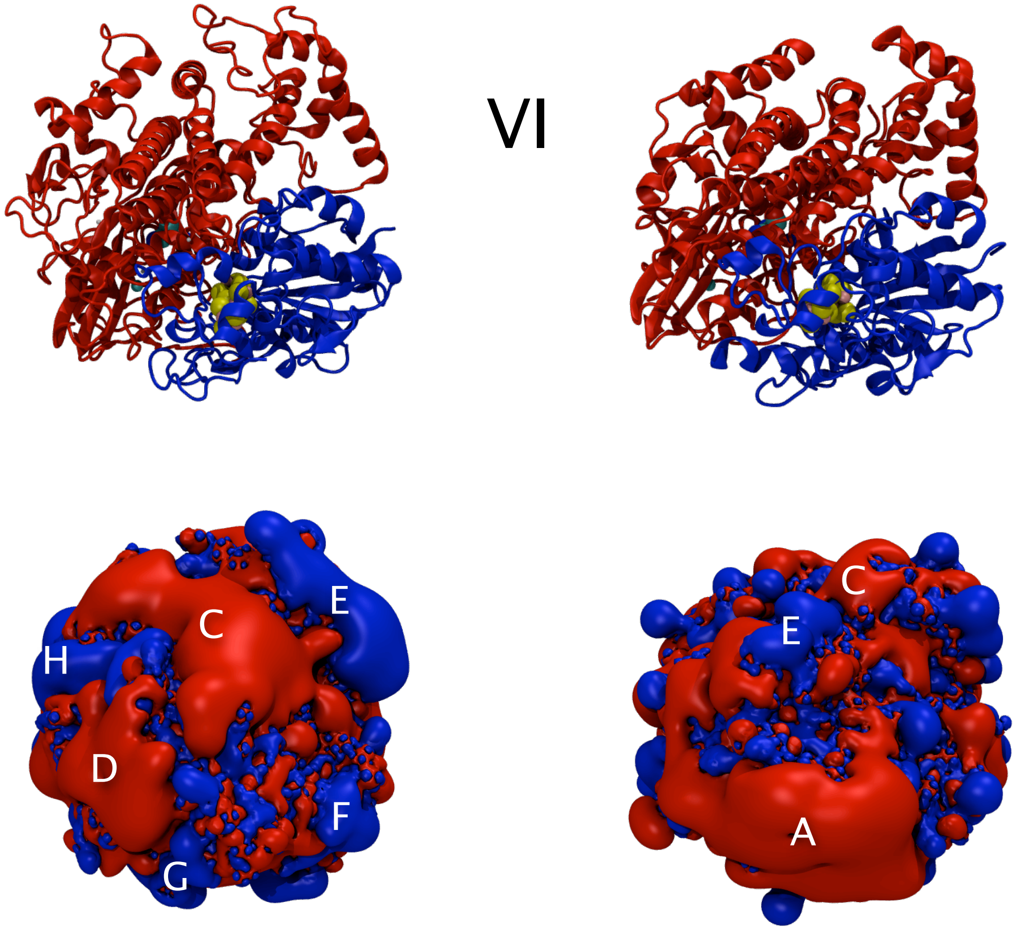
VI
E
C
H
D
F
G
C
E
A

Figure SI3

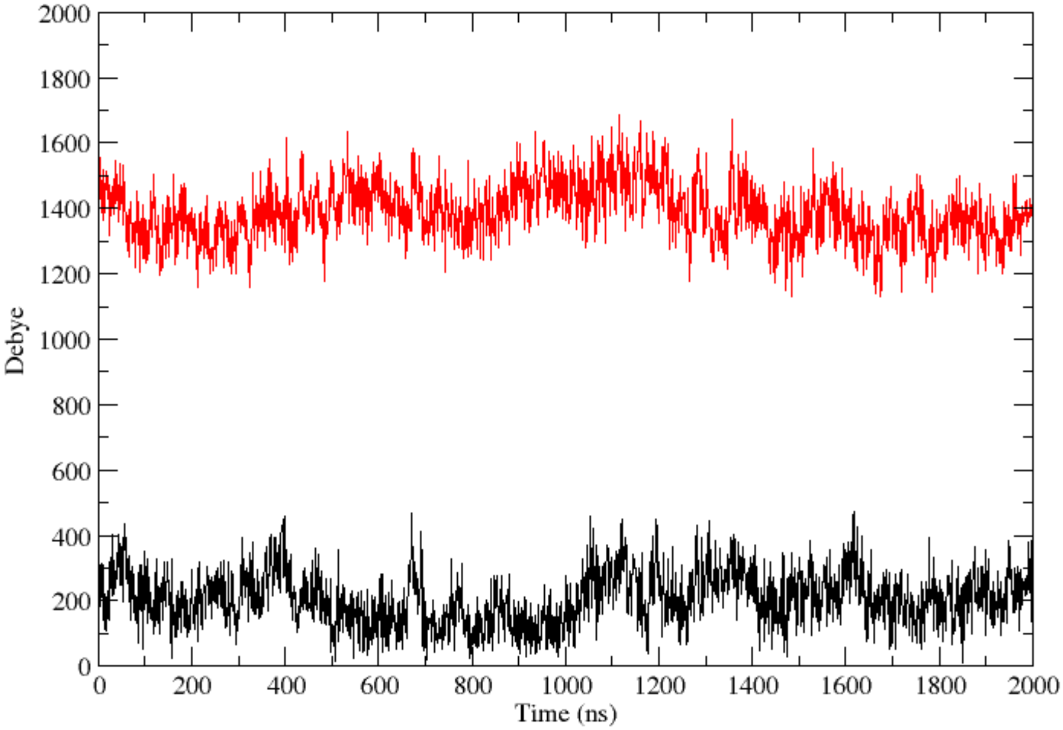

Figure SI4

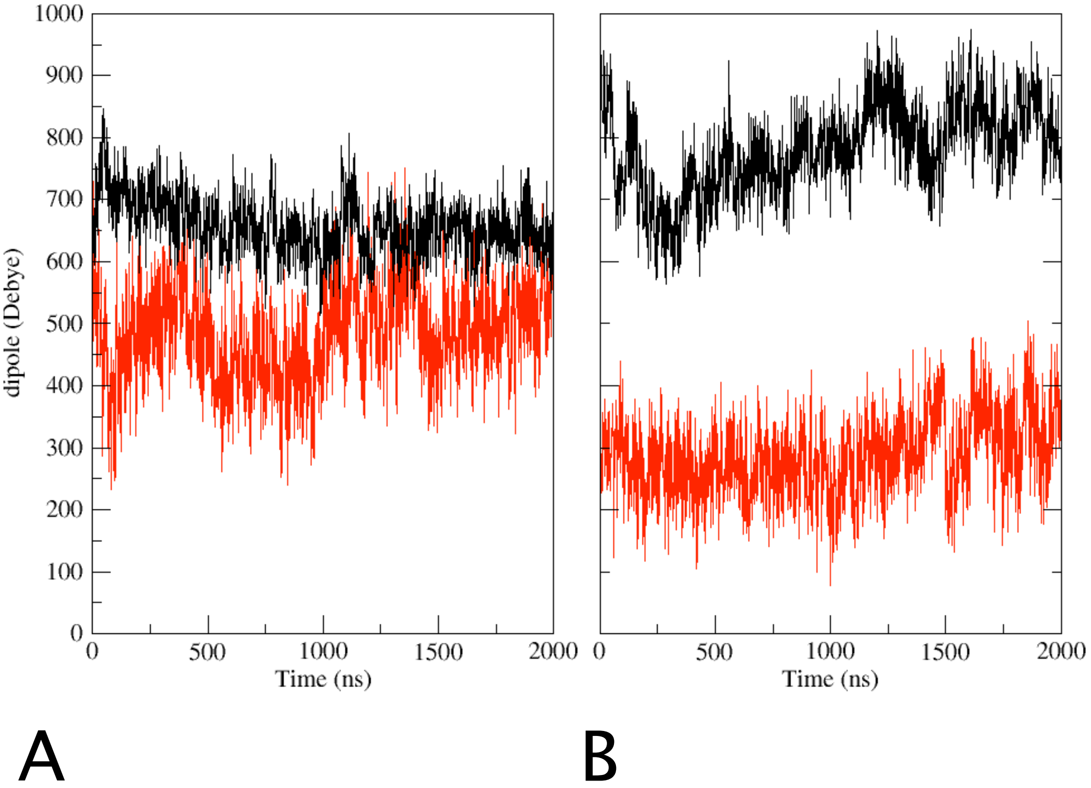
dipole (Debye)
0
100
200
300
400
500
600
700
800
900
1000
0
500
1000
1500
2000
Time (ns)
0
500
1000
1500
2000
Time (ns)
A
B

Fig. SI5

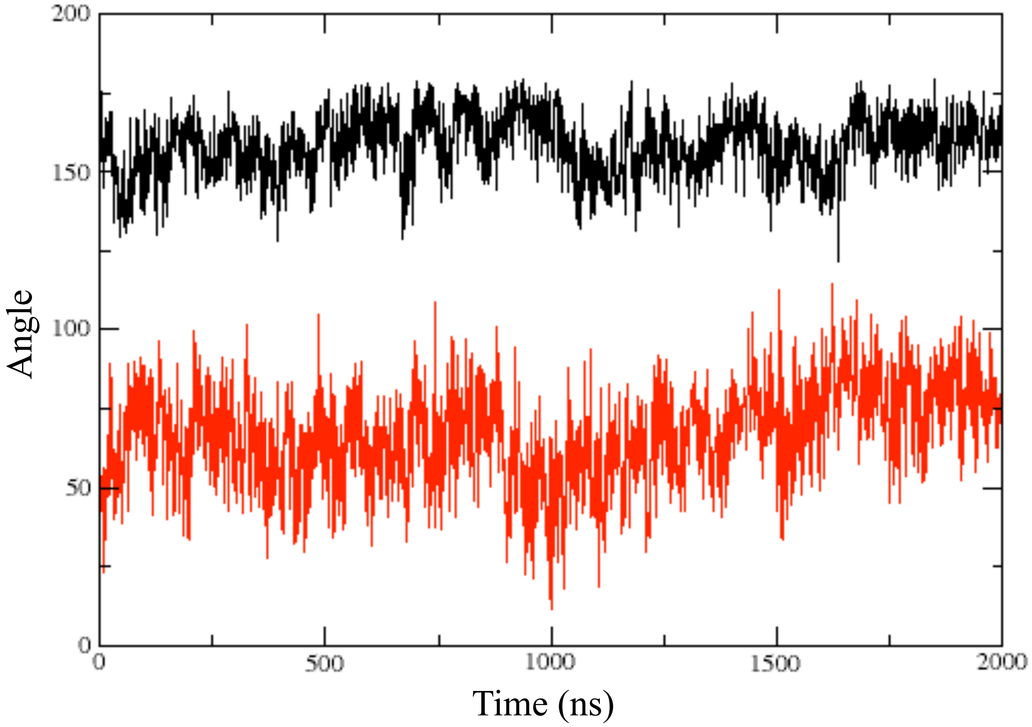

Figure SI6

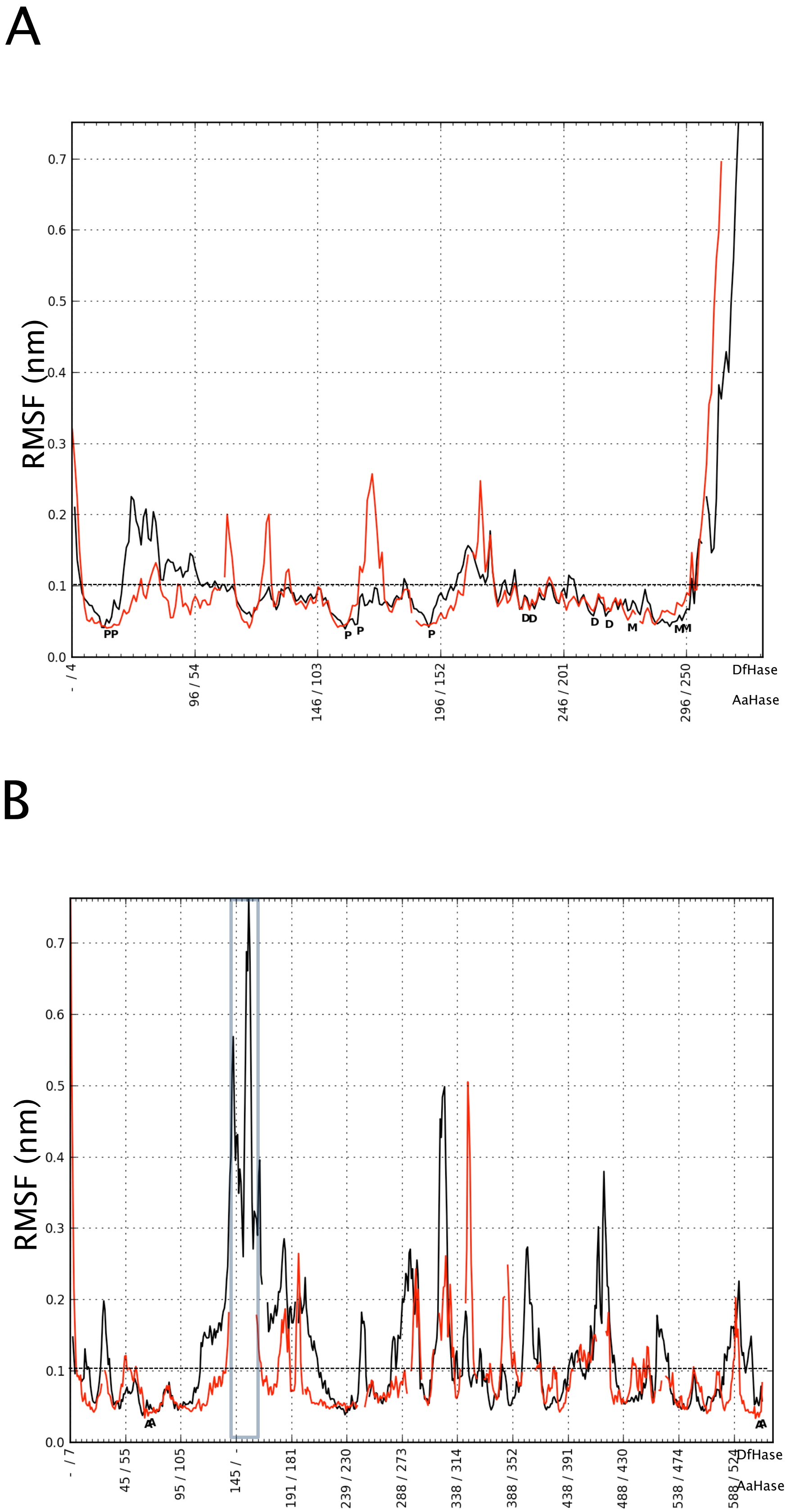
A
RMSF (nm)
0.0
0.1
0.2
0.3
0.4
0.5
0.6
0.7
- / 4
96 / 54
146 / 103
196 / 152
246 / 201
296 / 250
DfHase
AaHase
PP
P
P
P
DD
D
D
M
MM
B
RMSF (nm)
0.0
0.1
0.2
0.3
0.4
0.5
0.6
0.7
- / 7
45 / 55
95 / 105
145 / -
191 / 181
239 / 230
288 / 273
338 / 314
388 / 352
438 / 391
488 / 430
538 / 474
588 / 524
DfHase
AaHase
AA
AA